

# Resonance Energy Transfer and Superradiance Mediated by Plasmonic Nanowaveguides

Diego Martín-Cano,<sup>†</sup> Luis Martín-Moreno,<sup>‡</sup> Francisco J. García-Vidal,<sup>\*,†</sup> and Esteban Moreno<sup>\*,†</sup>

<sup>†</sup>Departamento de Física Teórica de la Materia Condensada, Universidad Autónoma de Madrid, E-28049 Madrid, Spain, and <sup>‡</sup>Instituto de Ciencia de Materiales de Aragón and Departamento de Física de la Materia Condensada, CSIC-Universidad de Zaragoza, E-50009 Zaragoza, Spain

**ABSTRACT** We show how both the subwavelength confinement associated with surface plasmons and the one-dimensional character of plasmonic waveguides can be exploited to enhance the coupling between quantum emitters. Resonance energy transfer and the phenomenon of superradiance are investigated in three different waveguiding schemes (wires, wedges, and channels) by means of the Finite Element Method. We also develop a simplified model that is able to capture the main features of the numerical results.

**KEYWORDS** Surface plasmons, quantum optics, energy transfer, superradiance

Controlling the radiation of atoms, molecules, or quantum dots is a hot topic in the current nanophotonics agenda. It is well-known<sup>1</sup> that the spontaneous decay rate of a single emitter can be enhanced or suppressed by careful modification of the photonic density of states accessible to the oscillating dipole. Optical nanoantennas are one example of structures providing such command.<sup>2</sup> When several sources are present, the emitted radiation can be exchanged among them. Depending on the distance between emitters and the directionality of radiation, various phenomena may occur, such as radiationless energy transfer,<sup>3</sup> radiative energy transfer,<sup>4</sup> and even the emergence of collective super- or subradiant states<sup>5</sup> with correspondingly altered emission rates. In the last decades, it has been demonstrated that metallic structures are a powerful mean to attain the above-mentioned control,<sup>6,7</sup> thanks to the high confinement of the surface plasmons (SPs) supported by them. In fact, due to their subwavelength character SPs are believed to be one of the best candidates to act as an intermediate between quantum emitters and light. Metallic nanospheres,<sup>8,9</sup> wires,<sup>10</sup> and more complex structures<sup>11</sup> have been considered to reach these goals, and strongly enhanced decay rates of quantum dots have been demonstrated with a view in future quantum plasmonic applications.<sup>12,13</sup> One further step consists in exploiting the one-dimensional character of waveguides to provide an intense coupling between two emitters.<sup>14</sup> In this report, we study the coupling of nanoscale emitters to various plasmonic waveguides to achieve plasmon-mediated energy transfer

and super- and subradiance. We numerically characterize realistic waveguides based on metallic wedges,<sup>15</sup> channels,<sup>16</sup> and wires, identifying those structures which are most promising for energy transfer and superradiance. In addition, the basic mechanisms behind their superior performance are explained.

**Resonance Energy Transfer.** In this section, we study the energy transfer between fluorescent molecules, known as Resonance Energy Transfer (RET). RET can proceed through various mechanisms. Forster (radiationless) energy transfer strongly decays with the distance between the molecules, and in vacuum it is most effective for distances smaller than about 10 nm. For larger distances, radiative transfer takes over, but the transfer rate in vacuum is nevertheless very small. It has been shown that the SPs arising in an environment consisting of a planar metallic film can enhance the transfer rate.<sup>7</sup> One of the goals of this report is to find out the extent to which coupling to plasmonic waveguides can increase the radiative transfer. Given both the one-dimensional character of the waveguides and the plasmonic field enhancement, an important improvement is expected. Similar ideas have been considered for dielectric<sup>14</sup> and slightly idealized metallic<sup>17</sup> waveguides. Here manufacturable plasmonic waveguides<sup>18</sup> with realistic properties are studied. The setup is displayed in Figure 1; an emitter (the donor) is positioned in the neighborhood of a metallic waveguide running along the *Z*-axis, and energy is transferred to a second molecule (the acceptor). Both molecules are located in the vertical symmetry *YZ*-plane at identical vertical height, *h*, and separated at a distance *d* along the waveguide. Silver circular cylinders, wedges, and channels are investigated here, whose properties are well described

\* To whom correspondence should be addressed. E-mail: (F.J.G.-V.) fj.garcia@uam.es; (E.M.) esteban.moreno@uam.es.

Received for review: 05/27/2010

Published on Web: 07/19/2010

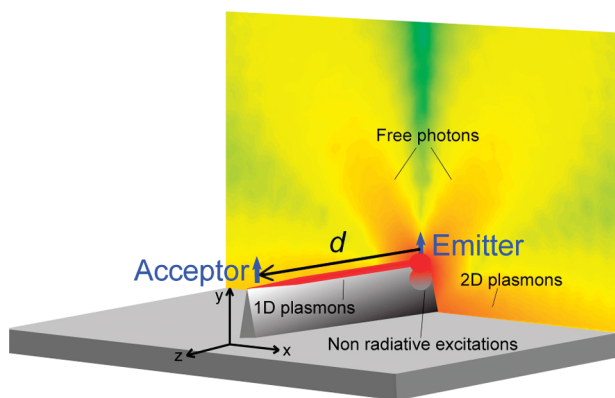


**FIGURE 1.** Diagram of the considered setup including the donor (emitter), acceptor, and plasmonic waveguide (a metallic wedge in this scheme). The various interaction channels are also schematically shown, including radiated photons, “radiated plasmons” (1D plasmons guided by the wedge and 2D plasmons supported by the horizontal metallic substrate), and nonradiative excitations in the metal in the neighborhood of the emitter.

in the literature.<sup>19–21</sup> The dielectric permittivity of silver at the operating wavelength,  $\lambda_0 = 600$  nm, is  $\epsilon_{Ag} = -13 + i0.8$ . We quantify the RET by the normalized energy transfer rate (nETR), that is, the energy transfer rate in the presence of the plasmonic waveguide normalized to that in vacuum, keeping the remaining factors (distances and dipole orientations) unchanged. The nETR is given by

$$\text{nETR} = \frac{\text{Im}[\mu_A^* \cdot \mathbf{G}(\mathbf{r}_A, \mathbf{r}_D) \cdot \mu_D]}{\text{Im}[\mu_A^* \cdot \mathbf{G}_{\text{vac}}(\mathbf{r}_A, \mathbf{r}_D) \cdot \mu_D]} \quad (1)$$

where  $\mu_D$  is the donor dipole moment vector positioned at  $\mathbf{r}_D$  (with analogous definitions for the acceptor, \* stands for complex conjugate),  $\mathbf{G}(\mathbf{r}, \mathbf{r}')$  is the Green’s tensor in the presence of the plasmonic waveguide (with similar definition for the case when both dipoles are in vacuum), and Im stands for the imaginary part. This expression can be also written as<sup>22</sup>

$$\text{nETR} = \frac{|\mathbf{n}_A \cdot \mathbf{E}_D(\mathbf{r}_A)|^2}{|\mathbf{n}_A \cdot \mathbf{E}_{D, \text{vac}}(\mathbf{r}_A)|^2} \quad (2)$$

where  $\mathbf{n}_A$  is a unit vector along the induced polarization of the acceptor (whose direction is assumed to be fixed), and  $\mathbf{E}_D(\mathbf{r}_A)$  is the electric field of the donor at the acceptor position in the presence of the plasmonic waveguide (with a similar definition when the dipoles are in vacuum). The electric fields involved in eq 2 are obtained by means of the Finite Element Method (COMSOL software), modeling the donor as a very short (2 nm) oscillating current. The upper panels of Figure 2 display the nETR as a function

of  $d$  and  $h$  for a circular cylinder (panel a), triangular wedge (panel b), and triangular channel (panel c). To have a meaningful comparison, the geometric parameters are such that the fundamental mode in all three waveguides has the same propagation length  $l = [2\text{Im}(k)]^{-1} = 1.7 \mu\text{m}$  with  $k$  being the complex modal wavevector. The geometry of the waveguides is summarized in the lower panels of Figure 2. Donor and acceptor are set with identical orientation, which is chosen so that it matches the dominant polarization of the plasmonic modes supported by the structures, that is, vertical ( $Y$ -axis) for the wire and wedge, and horizontal ( $X$ -axis) for the channel. For the range of distances  $d$  displayed in the figure, the nETR essentially grows with increasing donor–acceptor separations. This is because in vacuum the energy is spread in all three dimensions, whereas the presence of a waveguide provides a link between the locations of donor and acceptor. The dependence with the vertical coordinate,  $h$ , of the molecules is directly related to the corresponding plasmonic modal shapes. These mode profiles are rendered in the lower panels of Figure 2, as quantified by the amplitude of the transverse electric field normalized to the carried power. Thus, within the present framework, the nETR reaches its maximum at the metallic surface ( $h = 0$ ) for circular wires and wedges, whereas the optimal height is  $h = 35$  nm for channels. In absolute terms, the circular cylinder displays the lowest nETR, which is reasonable given its smaller field enhancement as compared with wedges and channels. In the range of  $d$  and  $h$  shown in Figure 2, wedges and channels feature nETRs up to  $3 \times 10^4$ , which is 20 times larger than the one corresponding to cylinders. Let us stress that when the separation  $d$  is fixed at, for example, half a wavelength, the nETR in the wedge can be strongly enhanced by letting  $h$  become smaller than 10 nm, reaching values higher than several tens of thousands. This enhancement is not possible for channels whose maximum achievable nETR is about 5000 for the above-mentioned  $d$ . The general conclusion is that the wedge is the most promising structure in terms of resonance energy transfer. It is possible to put some numbers to the efficiency of the resonance energy transfer mediated by plasmonic waveguides if we know this energy transfer rate in vacuum. Assuming that donor and acceptor molecules are characterized by a typical Forster radius,  $R_0 = 10$  nm, a simple calculation<sup>22</sup> predicts that the energy transfer rate of these two molecules when they are separated by a distance  $d = \lambda = 600$  nm in vacuum is about  $10^{-8}$  times the donor’s decay rate. Our calculations show that when donor and acceptor molecules are appropriately placed along a channel or a wedge plasmonic waveguide, that resonance energy transfer ratio can be increased up to  $10^{-4}$  for the considered distance.

The values of the nETR can be quantitatively explained with the following simplified model. The Green’s tensor

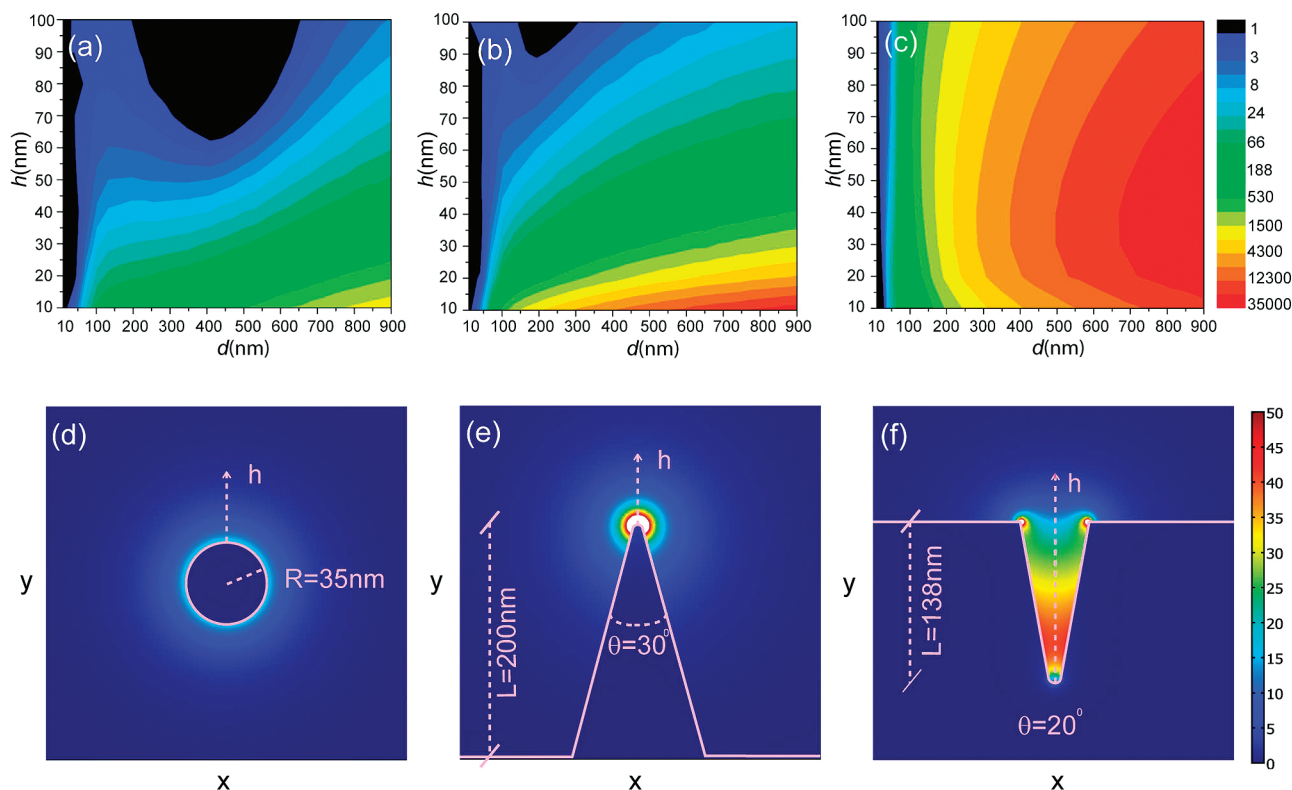


FIGURE 2. Normalized energy transfer rate (a–c) and modal shapes (d–f) for various plasmonic waveguides: circular wire (a,d), wedge (b,e), and channel (c,f). In the upper panels, the longitudinal separation between both dipoles is  $d$  (for its definition see Figure 1), and their vertical height is  $h$  (for their definitions see the lower panels). The lower panels display the geometry and the transverse electric field amplitude in the  $XY$ -plane, normalized to the guided power. The radius of curvature of the wedge tip is 5 nm.

appearing in eq 1 can be understood as the sum of several processes involving the excitation of waveguide modes, free space radiation, nonradiative absorption losses, and so on. A cartoon of the various channels in the case of a metallic wedge is suggested in Figure 1. If the waveguide is to play a major role, we can expect that the contribution to the Green's function stemming from the plasmonic guided mode is the most important one and neglect the remaining channels. Under this assumption and using the well-known expression for the Green's function in vacuum, one arrives to the following approximation for the nETR

$$\text{nETR} = \left(\frac{4\pi}{3}\right)^2 \left(\frac{\Gamma_{\text{guided}}}{\Gamma_{\text{vac}}}\right)^2 \exp\left(-\frac{d}{\lambda}\right) \left(\frac{d}{\lambda}\right)^2 \left[1 - \left(\frac{\lambda}{2\pi d}\right)^2 + \left(\frac{\lambda}{2\pi d}\right)^4\right]^{-1} \quad (3)$$

where  $\lambda$  is the vacuum wavelength,  $\lambda$  is the mode propagation length, and where we have  $\mathbf{n}_A = \mathbf{n}_D$ . In  $3\Gamma_{\text{guided}}$  is the spontaneous emission rate into guided plasmons by one single emitter in the presence of the plasmonic waveguide, and  $\Gamma_{\text{vac}}$  is the spontaneous emission rate of

photons by one single emitter in vacuum. When losses are not too high,  $\Gamma_{\text{guided}}$  can be computed as

$$\Gamma_{\text{guided}} = \Gamma_{\text{vac}} \frac{6\pi c \epsilon_0}{2k_0^2} \frac{|\mathbf{n}_D \cdot \mathbf{e}(\mathbf{r}_D)|^2}{\text{Re} \left[ \int dA \mathbf{z} \cdot (\mathbf{e}(\mathbf{r}) \times \mathbf{h}^*(\mathbf{r})) \right]} \quad (4)$$

where the meaning of the various symbols is the following:  $c$ ,  $\epsilon_0$ ,  $\mathbf{k}_0$  are the speed of light, permittivity, and wavevector in vacuum;  $\mathbf{e}(\mathbf{r})$ ,  $\mathbf{h}(\mathbf{r})$  are the electric and magnetic fields corresponding to the guided mode; the normalization integral in the denominator is extended to the transverse  $XY$ -plane; and  $\mathbf{z}$  is a longitudinal unit vector. Let us remark that  $\Gamma_{\text{guided}}$  is an  $h$ -dependent magnitude and its evaluation requires a separate 2D simulation of the guided mode fields. It is interesting to analyze the origin of the various factors in 3. Besides the geometric constant prefactor, the factor  $(\Gamma_{\text{guided}}/\Gamma_{\text{vac}})^2$ , which is independent of the donor–acceptor separation  $d$ , accounts for the typical decay rate enhancement due to the neighboring metallic structure. The exponential decay with  $d$  comes directly from the contribution of the plasmonic mode to the Green's function in the numerator of 1, and the remaining factors depending algebraically

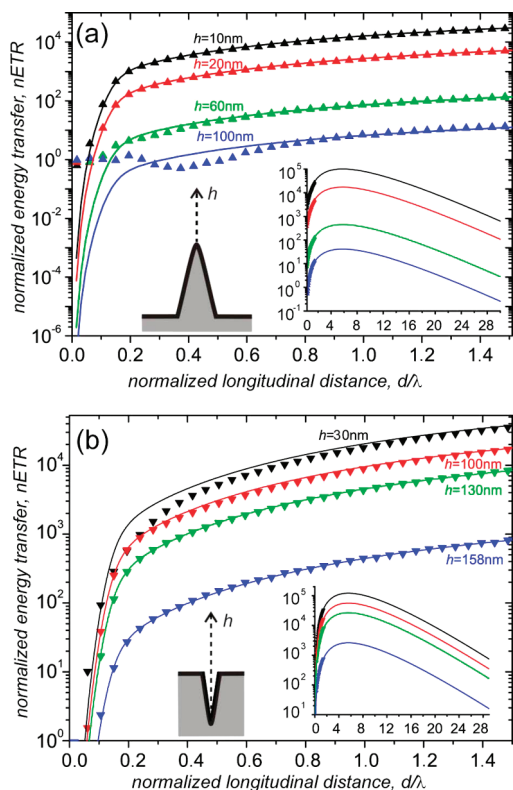


**FIGURE 3.** Normalized energy transfer rate between a donor and an acceptor as a function of their separation  $d$  for various heights  $h$ . (a) Wedge waveguide and (b) channel waveguide. The symbols correspond to numerical simulations, and the solid lines correspond to the simplified model described in the main text. The insets display the same magnitude for extended values of the abscissa.

on  $d/\lambda$  stem from the Green's function in vacuum, that is, the denominator of 1. Notice that the power coupled to the guided mode would keep propagating without decay for an ideal loss-free metal ( $\ell = \infty$ ), whereas the power emitted by the donor spreads in vacuum in the absence of the waveguide link. Thus, although an ideal (lossless) plasmonic guide would provide a monotonic growth of the nETR with  $d$  due to the vacuum normalization, realistic waveguides should display a maximum nETR with donor–acceptor separation. Figure 3 renders the nETR as a function of the donor–acceptor separation  $d$  normalized to  $\lambda$ , both numerically (symbols) and with the described model (solid lines), for various heights  $h$ . Panels a and b correspond to the wedge and the channel, respectively. Notice that all magnitudes in 3 are numerically computed so that there are no fitting parameters. The good concord between the numerical results and our simple model justifies the validity of our approximation. For wedges (panel a) the agreement only breaks down for small separations,  $d/\lambda < 0.6$ . This is most likely due to two reasons: (i) in this regime the contribution of radiative modes is not negligible and is superimposed to the guided mode contribution, and (ii) in the neighborhood of the donor location the fields present a spatial transient along

the longitudinal coordinate  $z$  and our simplified model, which includes only one single propagating mode, can obviously not reproduce this behavior. It is important to notice that our model allows one to explore energy transfer rates at donor–emitter separations, which are too large to be numerically modeled. The inset of Figure 3a displays the nETR for larger separations. The nETRs present maxima at  $d \approx 2\lambda$ , as can be easily obtained from 3, clearly showing that nETR grows only up to the point where absorption of the SP mode starts to dominate the picture. The interpretation is analogous for the channel waveguides.

**Super- and Subradiance.** Once we have demonstrated the enhancement of radiative energy transfer via plasmonic waveguide modes, it is natural to consider how the emission of two coupled sources evolves as a function of their separation. The cooperative emission rates of several coupled oscillating systems has been considered many times since the paper by Dicke,<sup>5</sup> including the recent all-optical analogue of two cavities connected by a photonic crystal waveguide,<sup>23</sup> and the effect of a metallic nanoparticle in the emission of an ensemble of dipoles.<sup>24</sup> Here, the goal is to study the coupling between two emitters mediated by a plasmonic waveguide. The considered waveguides, dipole orientations, and remaining parameters are identical to those in the previous section. However, in the results shown above the acceptor dipole moment was induced by the donor's field, whereas now both dipoles are emitters that interact and, as a consequence, the collective decay rate is modified. Although this is a new situation as compared with the previous section, the above-discussed results suggest nevertheless that a plasmonic waveguide should provide a very efficient coupling between the two emitters. Since wedge and channel waveguides feature a higher nETR, we focus now only on them. The dipole moments of both emitters are identical, they oscillate in phase, and are separated by a distance  $d$ . The contribution to the decay rate of an emitter with dipole moment  $\mu_i$  positioned at  $\mathbf{r}_i$  due to the presence of an emitter located at  $\mathbf{r}_j$  with dipole moment  $\mu_j$  is<sup>22</sup>

$$\Gamma_{ij} = \frac{4\omega^2}{\pi c^2 \epsilon_0 \hbar} \text{Im}[\mu_i^* \cdot \mathbf{G}(\mathbf{r}_i, \mathbf{r}_j) \cdot \mu_j] \quad (5)$$

where  $\omega$  is the angular frequency. For two dipoles coupled to a waveguide, the modification of the collective decay rate due to the presence of the second emitter is then quantified by the decay rate of the two interacting emitters divided by the sum of the decays of the emitters when they are alone and coupled to the waveguide. Because of symmetry ( $\Gamma_{11} = \Gamma_{22}, \Gamma_{12} = \Gamma_{21}$ ) this can be expressed as in the second equality

$$\gamma = \frac{\Gamma_{11} + \Gamma_{12} + \Gamma_{22} + \Gamma_{21}}{\Gamma_{11} + \Gamma_{22} + \frac{\text{Im}[\mu_1^* \cdot \mathbf{G}(\mathbf{r}_1, \mathbf{r}_1) \cdot \mu_1] + \text{Im}[\mu_1^* \cdot \mathbf{G}(\mathbf{r}_1, \mathbf{r}_2) \cdot \mu_2]}{\text{Im}[\mu_1^* \cdot \mathbf{G}(\mathbf{r}_1, \mathbf{r}_1) \cdot \mu_1]}} \quad (6)$$

This normalized decay factor has been numerically computed and it is rendered in Figure 4 for a wedge, (panel a), and a channel, (panel b). The symbols are the results of the Finite Element Method simulations. Whenever the normalized decay factor is larger (smaller) than 1, the system is superradiant (subradiant). The oscillations as a function of the normalized separation,  $d/\lambda$ , observed in both panels are due to the plasmonic coupling, its periodicity being twice the modal wavelength. This was to be expected because, since both dipoles oscillate in phase, this separation provides in-phase plasmonic driving. The amplitude of the oscillations is damped due to the lossy character of the plasmonic modes.

It is important to realize that the normalized decay factor,  $\gamma$ , depends in a nonmonotonic fashion with the vertical height of the emitters,  $h$ . Let us focus our attention on the maxima in Figure 4a occurring at  $d/\lambda = 0.8$ . It is observed that superradiance grows when the height increases from  $h = 10$  nm to  $h = 40$  nm, and then diminishes again when the height increases from  $h = 40$  nm to  $h = 100$  nm. Initially this seems to be at odds with the monotonic decrease of nETR as  $h$  is increased, displayed in Figure 3a. However, what is important in the present context is not the nETR but the fraction of photons that are coupled to guided plasmons. Indeed, for wedges the nETR grows when  $h$  is decreased, but at the same time the nonradiative losses in the neighborhood of the emitter dominate when  $h$  is smaller than about 5 nm, and this quenching reduces the plasmonic coupling between emitters. Therefore, the variation of  $\gamma$  with  $h$  should be controlled by the spontaneous emission  $\beta$  factor of 1 single emitter in the presence of the waveguide,  $\beta = \Gamma_{\text{guided}}/\Gamma_{11}$ . Our simplified model of the Green's tensor described in the previous section supports this view, since it predicts that the normalized decay factor of both emitters is given by

$$\gamma = 1 + \beta \cos(\mathbf{k}_r d) \exp\left(-\frac{d}{2\lambda}\right) \quad (7)$$

where  $\mathbf{k}_r = \text{Re}(\mathbf{k})$  is the real part of the complex wavevector of the plasmonic guided mode. Equation 7 is rendered with solid lines in Figure 4 for the chosen heights. Again the agreement between the simplified model and the simulations is very good, except for small separations, for the same reasons detailed in the previous section. To pin down our explanation, the  $\beta$ -factor has been computed

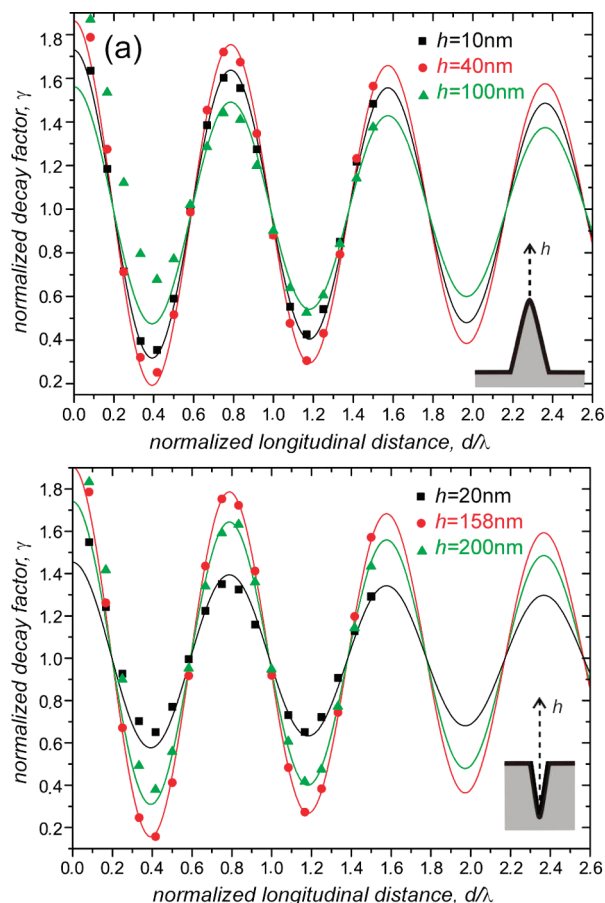
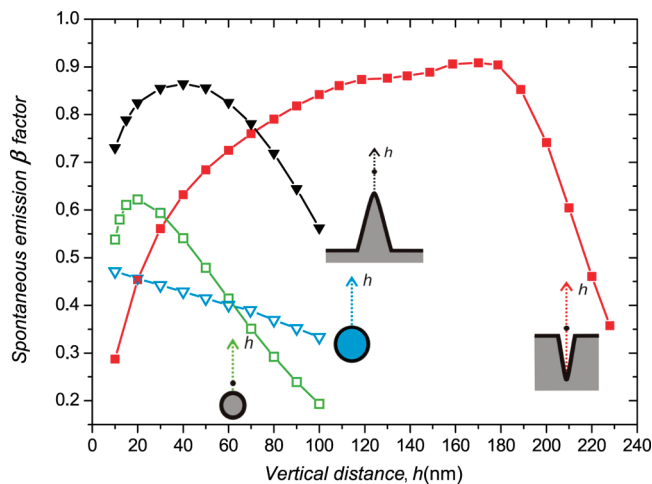


FIGURE 4. Normalized decay factor of 2 emitters coupled by a plasmonic waveguide as a function of their separation  $d$ , for various heights  $h$ . (a) Wedge waveguide and (b) channel waveguide. The symbols correspond to numerical simulations, and the solid lines correspond to the simplified model described in the main text.

and plotted as a function of the vertical height  $h$  in Figure 5 for several waveguides. The black line (triangles) corresponds to a wedge waveguide, and a maximum is indeed observed for  $h = 40$  nm, in accordance with the above-mentioned nonmonotonic behavior observed in Figure 4a. In a similar way the  $\beta$ -factor for the channel waveguide (Figure 5, red squares) presents a maximum when the emitter is slightly outside the channel ( $h = 158$  nm), fitting the behavior observed in Figure 4b. It is important to emphasize that it is our simplified model that demonstrates the relevance of the plasmonic guided modes and allows us to estimate that the coupling may be large even for separations,  $d$ , larger than a few wavelengths. The channel waveguide stands out as the best of the structures considered here, both because it has the largest maximum  $\beta$  factor ( $\beta \approx 0.9$ ), and because it features a broader  $h$ -range where the  $\beta$  factor remains high. Therefore it would be better for cases when the vertical position of the dipole is not well controlled. Figure 5 also renders  $\beta$ -factors for metallic and dielectric circular



**FIGURE 5.** Spontaneous emission  $\beta$ -factor of 1 emitter in the neighborhood of a plasmonic waveguide as a function of its height  $h$ . Black triangles (wedge waveguide), red solid squares (channel waveguide), green open squares (circular metallic wire), blue open triangles (dielectric circular wire). The metallic waveguides have the same parameters as described in Figure 2. The small black dots in the insets correspond to the locations where  $\beta$  is maximum. The dielectric wire has radius 50 nm and permittivity  $\epsilon = 15$ .

wires, showing that even for the most favorable  $h$  they are less apt for the present purpose, reaching at most  $\beta \approx 0.6$ .

In conclusion, we have studied resonance energy transfer and superradiance assisted by plasmonic waveguides in realistic and manufacturable structures using the Finite Element Method. The main features of both phenomena are well described by a simplified model that takes into account the plasmonic coupling and neglects the remaining interaction processes. We demonstrate that a metallic wedge is suited for donor–acceptor energy transfer, whereas a metallic channel is more appropriate for the coupling of two emitters. The proposed control of the radiative properties of nanosources and enhanced resonance energy transfer has important applications such as sensing or single-atom spectroscopy. In addition, the high  $\beta$  factors in wedges and channels suggest that they may be interesting for the design of very efficient single-plasmon sources. Moreover, the achieved plasmonic-mediated interaction and superradiance can be employed to strongly couple the emitters at separations much larger than the involved optical wavelength. This large-separation strong coupling would be impossible in vacuum or with a dielectric fiber and is very promising to produce entangled states of two quantum emitters.<sup>25</sup>

**Acknowledgment.** This work has been sponsored by the Spanish Ministry of Science under Projects MAT2009-06609-C02 and CSD2007-046-NanoLight. D.M.C. acknowledges funding from the Spanish Ministry of Education under Grant FPU AP2007-00891.

## REFERENCES AND NOTES

(1) Purcell, E. M. Spontaneous emission probabilities at radio frequencies. *Phys. Rev.* **1946**, *69*, 681.

(2) Bharadwaj, P.; Deutsch, B.; Novotny, L. Optical antennas. *Adv. Opt. Photonics* **2009**, *1*, 438.

(3) Forster, T. Zwischenmolekulare Energiewanderung und Fluoreszenz. *Ann. Phys.* **1948**, *2*, 55.

(4) Marocico, C. A.; Knoester, J. Intermolecular resonance energy transfer in the presence of a dielectric cylinder. *Phys. Rev. A* **2009**, *79*, No. 053816.

(5) Dicke, R. H. Coherence in spontaneous radiation processes. *Phys. Rev.* **1954**, *93*, 99.

(6) Ford, G. W.; Weber, W. H. Electromagnetic interactions of molecules with metal surfaces. *Phys. Rep.* **1984**, *113*, 195.

(7) Andrew, P.; Barnes, W. L. Energy Transfer Across a Metal Film Mediated by Surface Plasmon Polaritons. *Science* **2004**, *306*, 1002.

(8) Anger, P.; Bharadwaj, P.; Novotny, L. Enhancement and Quenching of Single-Molecule Fluorescence. *Phys. Rev. Lett.* **2006**, *96*, 113002.

(9) Kuhn, S.; Hakanson, U.; Rogobete, L.; Sandoghdar, V. Enhancement of Single-Molecule Fluorescence Using a Gold Nanoparticle as an Optical Nanoantenna. *Phys. Rev. Lett.* **2006**, *97*, No. 017402.

(10) Chen, Y.; Nielsen, T. R.; Gregersen, N.; Lodahl, P.; Mork, J. Finite-element modeling of spontaneous emission of a quantum emitter at nanoscale proximity to plasmonic waveguides. *Phys. Rev. B* **2010**, *81*, 125431.

(11) Tamini, T. H.; Stefani, F. D.; van Hulst, N. F. Enhanced directional excitation and emission of single emitters by a nano-optical Yagi-Uda antenna. *Opt. Express* **2008**, *16*, 10858.

(12) Akimov, A. V.; Mukherjee, A.; Yu, C. L.; Chang, D. E.; Zibrov, A. S.; Hemmer, P. R.; Park, H.; Lukin, M. D. Generation of single optical plasmons in metallic nanowires coupled to quantum dots. *Nature* **2007**, *450*, 402.

(13) Kolesov, R.; Grotz, B.; Balasubramanian, G.; Stohr, R. J.; Nicolet, A. A. L.; Hemmer, P. R.; Jelezko, F.; Wrachtrup, J. Wave-particle duality of single surface plasmon polaritons. *Nat. Phys.* **2009**, *5*, 470.

(14) Kien, F. L.; Dutta Gupta, S.; Nayak, K. P.; Hakuta, K. Nanofiber mediated radiative transfer between two distant atoms. *Phys. Rev. A* **2005**, *72*, No. 063815.

(15) Boltasseva, A.; Volkov, V. S.; Nielsen, R. B.; Moreno, E.; Rodrigo, S. G.; Bozhevolnyi, S. I. Triangular metal wedges for subwavelength plasmon-polariton guiding at telecom wavelengths. *Opt. Express* **2008**, *16*, 5252.

(16) Bozhevolnyi, S. I.; Volkov, V. S.; Devaux, E.; Laluet, J.-Y.; Ebbesen, T. W. Channel plasmon subwavelength waveguide components including interferometers and ring resonators. *Nature* **2006**, *440*, 508.

(17) Dzsotjan, D.; Sorensen, A. S. Fleischhauer, M. Quantum emitters coupled to surface plasmons of a nano-wire: A Green function approach. arXiv:1002.1419v2.

(18) Bozhevolnyi, S. I. *Plasmonic Nanoguides and Circuits*; World Scientific: Singapore, 2009.

(19) Takahara, J.; Yamagishi, S.; Taki, H.; Morimoto, A.; Kobayashi, T. Guiding of a one-dimensional optical beam with nanometer diameter. *Opt. Lett.* **1997**, *22*, 475.

(20) Moreno, E.; Rodrigo, S. G.; Bozhevolnyi, S. I.; Martin-Moreno, L.; Garcia-Vidal, F. J. Guiding and Focusing of Electromagnetic Fields with Wedge Plasmon Polaritons. *Phys. Rev. Lett.* **2008**, *100*, No. 023901.

(21) Moreno, E.; Garcia-Vidal, F. J.; Rodrigo, S. G.; Martin-Moreno, L.; Bozhevolnyi, S. I. Channel Plasmon Polaritons: modal shape, dispersion, and losses. *Opt. Lett.* **2006**, *31*, 3447.

(22) Novotny, L.; Hecht, B. *Principles of Nano-Optics*; Cambridge University Press: Cambridge, U.K., 2006.

(23) Pan, J.; Sandhu, S.; Huo, Y.; Stuhmann, N.; Povinelli, M. L.; Harris, J. S.; Fejer, M. M.; Fan, S. Experimental demonstration of an all-optical analogue to the superradiance effect in an on-chip photonic crystal resonator system. *Phys. Rev. B* **2010**, *81*, No. 041101(R).

(24) Pustovit, V. N.; Shahbazyan, T. V. Cooperative emission of light by an ensemble of dipoles near a metal nanoparticle: The plasmonic Dicke effect. *Phys. Rev. Lett.* **2009**, *102*, No. 077401.

(25) Chen, G.-Y.; Chen, Y.-N.; Chuu, D. S. Spontaneous emission of quantum dot excitons into surface plasmons in a nanowire. *Opt. Lett.* **2008**, *33*, 2212.